applied sciences

MDPI

Article

# 3D Surgical Planning for Customized Devices in Orthopaedics: Applications in Massive Hip Reconstructions of Oncological Patients

**Yazan Haidar [1,2], Claudio Belvedere [2,*], Benedetta Spazzoli [3], Davide Maria Donati [3] and Alberto Leardini [2]**

[1] Biomedical Engineering, University of Glasgow, Glasgow G12 8QQ, UK; yazanbaseem.001@gmail.com
[2] Laboratory of Movement Analysis and Functional Evaluation of Prosthesis, IRCCS Istituto Ortopedico Rizzoli, 40136 Bologna, Italy; leardini@ior.it
[3] Department of Orthopaedic Oncology, IRCCS Istituto Ortopedico Rizzoli, Via Pupilli 1, 40136 Bologna, Italy; benedetta.spazzoli@ior.it (B.S.); davidemaria.donati@ior.it (D.M.D.)
* Correspondence: belvedere@ior.it; Tel.: +39-051-6366570

**Abstract:** This study investigates the morphological impact of using three-dimensional (3D) printed custom implants in surgical hip reconstruction compared to the conventional bone graft and standard size implant methods. An amount of 16 patients at the Rizzoli Orthopaedic Institute who underwent hip reconstruction surgery for tumors involving the P2 pelvis region were selected using stratified sampling. Half of them were randomly selected to receive 3D-printed implants, and the other half were selected to receive standard implants with bone grafts. Six months post-surgery, computed tomography (CT) scans were used to identify the hip joint center of rotation and to measure greater the trochanter offset and acetabular inclination angle. These CT scans were also used to construct a 3D model of the pelvis for 3D measurements. The results show no significant differences in accuracy, using Student's *t*-test and Mann–Whitney U-test ($p$-value > 0.05), between the two methods for reconstructing the hip joint center of rotation or greater trochanter offset. However, 3D-printed implants showed statistically significant greater precision, using Student's *t*-test ($p$-value < 0.05), in reconstructing the acetabular inclination angle compared to the conventional bone graft and standard-sized off-the-shelf implants. This superior precision reduces the risk of impingement of the femur implant neck with the acetabulum implant cup, which directly relates to improved implant survivorship. These findings support the continued exploration of 3D printing technology for personalized orthopedic solutions.

**Keywords:** hip joint reconstruction; 3D printing; custom implants; morphological analysis; 3D; virtual measurement; massive bone loss; additive manufacturing; computer aided design; precision; accuracy

check for updates

**Citation:** Haidar, Y.; Belvedere, C.; Spazzoli, B.; Donati, D.M.; Leardini, A. 3D Surgical Planning for Customized Devices in Orthopaedics: Applications in Massive Hip Reconstructions of Oncological Patients. *Appl. Sci.* **2024**, *14*, 11054. https://doi.org/10.3390/app142311054

Academic Editor: Francesco Cappello

Received: 20 September 2024
Revised: 26 October 2024
Accepted: 25 November 2024
Published: 27 November 2024



## 1. Introduction

The use of 3D printing has found extensive applications in a variety of major industries and in healthcare [1–3]. In drug manufacturing, 3D printing has been used to make personalized drug products [4]. In orthopedics, it has revolutionized the way surgical procedures are carried out. Its impact extends to, but is not limited by, 3D printing anatomical models used for training, patient-specific surgical instruments, producing of prostheses with additive manufacturing, and production of customized 3D-printed implants [5]. Evidently, this technology has already proved its usefulness in a wide range of applications. By utilizing advanced medical imaging techniques, such as CT scans and magnetic resonance, surgeons are able to create accurate 3D models of the patient's anatomy, including bones, muscles, and tendons. These models provide a comprehensive visualization of the patient's unique condition, allowing for medical education, precise pre-operative planning and simulation, as well as execution [6–8]. Three-dimensional printing has been shown to improve surgical outcomes by enabling the personalization and customization of implants [5,9]. For example, when it comes to pelvic reconstruction following massive bone loss in oncological cases, allograft reconstruction is considered the gold standard [10] due to its effectiveness [11,12]. It involves using bone grafts from a bone bank or the patient to restore pelvic bone structure, although complications like non-union and fractures are common [13–15]. It is worth noting that while allografts offer an advantage over autografts, such as avoiding donor site morbidity, they suffer from weakened mechanical properties as a result of the sterilization and storage processes [16]. An alternative option is allograft–prosthetic composite reconstruction, such as saddle endoprosthesis, but this shows poor clinical results [17] and comparatively fewer superior outcomes than custom implants [18]. Traditional off-the-shelf implants may not always fit perfectly with the patient's anatomy. Finally, arthrodesis, a procedure that fuses the joint for stability and pain relief, is used when joint preservation is not possible. This results in loss of joint motion and has a 60% rate of non-union [19].

Other advanced technologies have had a positive impact on orthopedic surgery, such as the use of robotic surgery and computer navigation systems. The former has been found to enable more accurate implant placement compared to a manual approach [20]. However, this does not overcome the mismatch in design and size between standard implants and native bone anatomy. The latter's initial implementation improved oncological results through enhanced tumor resection planning by identifying clear resection margins at the surgical planning stage, and was further developed to enable 3D surgical planning by recreating the target patient's anatomy [21]. While it improves resection accuracy, this too does not address the mismatch in design and size between standard implants or bone grafts and native bone anatomy.

While there are several reports on the general clinical impact of 3D-printed customized implants [10,22,23], there are a lack of morphological studies on its impact on pelvic reconstruction accuracy and precision. That is why, in this study, the impact of 3D printing in hip reconstruction will be investigated by measuring objective positional parameters that are indicative of surgical success and can be compared with the conventional procedure of using bone graft and standard off-the-shelf implants for reconstruction. This will delineate the exact impact factors that are influenced by 3D-printed custom implants.

There is a multitude of etiologies that lead to massive bone loss [24] and thus demand complex reconstruction in the pelvis, such as reconstruction following tumor resection [11,12,25], trauma [26], and revision and re-revision surgeries following total hip arthro-plasties. In response to these procedures, there are currently several surgical procedures that are used for effective reconstruction. Some of the most common procedures are pure allograft reconstruction [13,27–29], allograft-prosthetic composite reconstruction [30,31], and arthrodesis [19]. While these procedures have their unique advantages, they also come with some inherent limitations. As such, there is no clear procedure that stands out. Because of this, the development of a reconstruction procedure using custom 3D-printed mega-prosthesis has occurred, which already has some good indications for such cases of massive bone loss [32].

Previous studies indicate that 3D-printed custom implants offer an effective strategy for complex pelvic reconstruction after tumor resection, showing acceptable functional outcomes and prosthesis survival rates. One study reported a median Musculoskeletal Tumor Society score of 63.3% and a survival rate of 73.3% at 33.8 months follow-up [22]. A second study found an average Musculoskeletal Tumor Society score of 46.3% and a 5 year survival rate of 85.7% [10]. A third study reported a mean Musculoskeletal Tumor Society score of 72% and a 3 year prosthesis survival rate of 69% [23].

Existing research into the effects of 3D-printed custom implants on hip surgery is mainly focused on clinical and functional criteria, such as Oxford Hip Score, Harris hip score, aseptic loosening, dislocation, formation of cracks, and nerve injuries [9,33–36]. However, there seems to be a lack of research on the morphological analysis of custom 3D-printed implants in comparison with conventional procedures. That is why, after an extensive review of the published research, a set of the most revealing morphological parameters of surgical success have been delineated, the first being the hip joint center of rotation, which is defined as the femur head center. While there are published morphological analyses of pelvic reconstructions, such as on the hip center position and its influence on functional outcomes [37,38], these do not include surgeries with 3D-printed custom implants. However, they do highlight that this position has the most significant impact on kinematics, such as on the range of hip joint motion. Additionally, deviations in the position of the hip center of rotation can impact the bio-mechanics of the pelvis during loading. This disrupts pelvic load transmission and thus generates stress concentrations that can increase the chance of implant mechanical failure in the long run [39]. That is why hip joint center position is taken as the primary parameter in the present analysis.

The greater trochanter offset is the distance from the femur head center to the greater trochanter [40]. The greater trochanter is the epiphysis for insertion of the main abductor muscles, gluteus medius and minimus; it extends the femur neck and shaft junction [41–43]. In addition, the piriformis muscles insert into the tip of the greater trochanter. It is part of the muscle group which activates to perform a hip extension and external rotation [44]. Inaccurate restoration of the greater trochanter offset after surgery, such that it does not match the healthy contra-lateral side, has been found to be a cause of pain in the abductor muscle due to increased tension, required to maintain the pelvis balanced [43], as a cause of increased wear of the implant articulating surface, and as a cause of inferior patient-reported outcomes [45,46]. Finally, this parameter indicates how satisfactory the lower limb length has been restored [47].

The acetabular inclination angle is the angle measured in the frontal plane between the normal acetabular ridge plane and the longitudinal axis of the patient [48]. An optimal inclination angle causes a better outcome for the functioning of the joint. Maintaining an angle lower than 45 degrees was found to avoid implant wear [49–52], thus elongating the lifetime of the implant, as well as minimizing joint impingement [53]. The decreased wear of an accurately reconstructed acetabular inclination angle could be due to the greater contact area between the femoral head and acetabular cup, which leads to reduced contact stresses, as compared to inaccurate reconstruction, which lowers this contact area [54]. The reason this parameter is needed is because, in terms of wear, the hip center position has no impact.

There are three main aims for this study: first, develop a reliable data processing workflow starting from medical image acquisition to final data analysis; second, assess the intra-patient accuracy of pelvic reconstruction within the conventional bone graft group and the 3D-printed customized implant group; third, compare the precision of reconstruction of the pelvis between the conventional bone graft procedure and the 3D-printed customized implant procedure.

## 2. Materials and Methods

The use of customized 3D-printed implants in the present study was approved by the Institutional Review Board (Prot. BACINOCUSTOM (2014)—CE AVEC ID: EM468/2021_47/2014/Oss/IOR_EM1) for studies involving humans. This study was conducted in accordance with the Declaration of Helsinki. All of the patients gave written informed consent for the procedure.

Patients with pelvis bone tumors were operated at the Rizzoli Orthopedic Institute. They all underwent massive hip reconstruction, including a type 2 tumor resection (Figure 1), as per Enneking's classification of pelvic resections [55]. They all shared the need for the complete reconstruction of the hip joint. A total of 17 patients were randomly divided into two groups; one patient was excluded for low-resolution post-operation CT scans (slice thickness > 2 mm) which prevented the 3D-model reconstruction for subsequent analysis. This is because the CT scans for that patient were carried out using settings for clinical assessment at the 6 month follow-up rather than for morphological analysis. Future scans intended for morphological analysis must adhere to the required scan settings. Ultimately, eight patients (female/male: 4/4; age: 32.2 $\pm$ 8.0; Body Mass Index:

22.0 ± 3.0 kg/m$^2$) had received a customized 3D-printed implant, and the other eight patients (female/male: 3/5; age: 42.8 ± 9.8; Body Mass Index: 21.0 ± 3.2 kg/m$^2$) received bone grafts in combination with standard off-the-shelf acetabular and femoral components (CLS stem/acetabular component, Zimmer GmbH, Winterthur, Switzerland). The second group represents the conventional procedure for these clinical cases, and thus serves as a benchmark for 3D-printed custom implants.

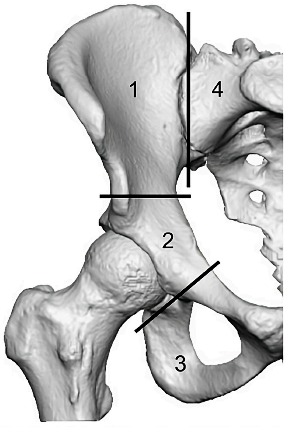


**Figure 1.** Enneking's tumor resection classification [22].

Both the custom-made 3D-printed implant, as well as the relevant surgical instruments, are in line with the European Directive requirements 93/42/EEC [56]. The implants were manufactured by Waldemar Link GmbH and Co. KG, Hamburg, Germany, using a medical grade titanium–aluminum–vanadium alloy (Ti6Al4V), which is in conformation with "The International Organization for Standardization" (ISO) 5832/3 and "American Society for Testing and Materials" F136 [57,58]. The custom implants were made using electron beam melting, an innovative 3D-printing method. This follows an iterative process which first starts by creating a vacuum in the chamber, then spreads a layer of the chosen metal powder on the printer bed. The electron beam is then aimed at the desired locations to bombard the electrons with the metal, which generates extreme heat high enough to melt and fuse the metal powder. The print bed is lowered and another fresh layer of metal is spread on the surface. This is repeated until the part is complete. Electron beam sintering uses a vacuum to eliminate any particles that would bombard the electrons and thus deviate them from the target location in the powder.

Titanium was chosen since recent advancements in 3D-printing technologies have enabled it to be used as a bio-compatible metal [22] and because it is found to promote osseointegration [59] better than cobalt–chromium [60]. The 3D-printed implants were based on 3D digital models designed for the specific 3D anatomical models of patient pelvises, obtained from a pre-op CT. Additionally, a 700 micron lattice was made in areas in direct contact with bone that is intended for fusion. The lattice creates a perfect trabecular root, thus bolstering secondary osseointegration as well as nearing the mechanical strength of the surrounding bone.

Patients then underwent another CT scan at their 6 month follow-up (Figure 2). Those scans, stored in the form of Digital Imaging and Communications in Medicine files, were segmented using Mimics Innovation Suite (Materialise NV, Leuven, Belgium) to form the 3D anatomical models. No inflammatory reactions or other side effects were observed in this follow-up period after surgery.

Segmentation on mimics relies on thresholding, which plays a pivotal role in accurately distinguishing bone tissue from the surrounding structures within the CT images. An appropriate selection of the Hounsfield Unit (HU) threshold, typically within the lower end of the spectrum at around 400 HU, using Mimics' thresholding tool, was used for non-bone tissue elimination. This threshold value directly influences model quality, as it dictates the differentiation between bone and non-bone pixels. Striking a balance between minimizing model noise and maximizing bone model completeness while preserving anatomical fidelity is crucial. An excessively low threshold can introduce unwanted noise, while an overly high threshold risks generating incomplete models with significant gaps. In every case, subsequent refining of the bone models is carried out.

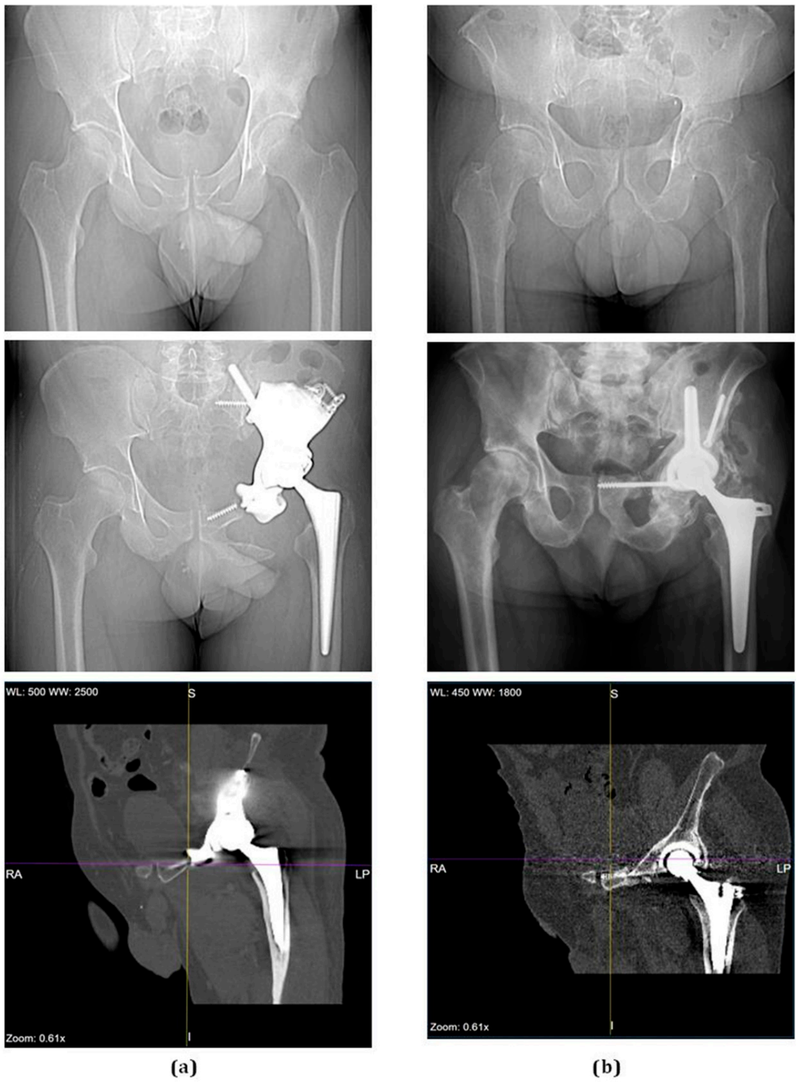


**Figure 2.** Radiological examination of two representative patients, one selected for a 3D-printed custom implant (**a**) and one for the bone graft implant (**b**). Pre-operative frontal radiograph (top images), post-operative frontal radiograph at 6 month follow-up (middle images), and CT scan (bottom images). Notice how the CT in (**a**) has a larger area of high signal intensity in the pelvis, which represents the massive pelvic implant compared to the CT in (**b**) with a smaller area of signal intensity representing the acetabular cup and bone graft in the pelvis.

The bone-model refining process begins after forming a preliminary 3D bone model, with the next step being the isolation of individual bones, including the left and right pelvic girdles, left and right femurs, and the sacrum. To achieve this, the split mask tool is employed, which involves manually identifying the boundaries between adjacent bones on 2D CT slices across the frontal, sagittal, and transverse planes. This tool traces bone boundaries based on each pixel's HU value, guided by the manually marked lines. In cases where metal implants cause noise similar in intensity to the bone, as seen in areas like the acetabulum–femur head and pelvic girdle–sacrum regions, precise slice-by-slice boundary marking is essential for creating an accurate bone model.

Once the bones are isolated, there may be gaps in the contour that need to be filled. For smaller gaps, the smart fill tool is used to automatically merge nearby pixels, with adjustments made based on the sharpness of the bone features. Sharper features, like the femur head, require a smaller-radius brush, while smoother areas need a larger-radius brush. More-complex gaps are filled with the edit mask tool, which operates on a slice-by-slice basis. The multi-slice edit tool is also employed for non-complex gaps, using interpolation across slices to close gaps while potentially overlooking intricate details. Typically, the multi-slice tool is used first for general modifications, followed by the edit mask tool for more precise refinements. Alternating between these tools helps ensure that both large and small features are preserved.

However, as a result of the excess noise from the metal implant in the femur, which completely merges the noise with the surrounding bone, it is still impossible to segment the greater trochanter on Mimics innovation suite. That is why greater trochanter recreation is carried out on the side of the implant. Greater trochanter recreation makes use of the healthy femur and the feature-based alignment tool available from Geomagic Control 2014.3.0 (3D Systems, Rock Hill, SC, USA). First, a copy of the healthy femur is made and is mirrored, given the bilateral symmetric nature of the human anatomy. Then, the shaft of the femur is selected, and a best-fit cylinder is created. This built-in feature of the software uses a least-squares algorithm to ensure that the positioned cylinder is in the closest orientation to all of the points in the selected area. The least-squares algorithm finds the position that minimizes the sum of the squared errors, where the errors are the differences between the selected data points and those of the geometrical shape. This is used to create an anatomical axis to be used for planning the alignment. Following that, the lesser trochanter is selected, and a best-fit sphere is positioned on it using the same algorithm. This built-in feature of the software uses the least-squares algorithm to ensure that the positioned sphere is in the closest orientation to all of the points in the selected area. This is used to create a point of coincidence between the lesser trochanters of both femurs. The same is then repeated for the original affected femur. Finally, the feature-based alignment tool is used. It works by overlapping the test object on the stationary object through the use of a matching pair of features on each. In this case, the original affected femur is set as the reference object, which remains stationary, and the mirrored healthy femur is set as the test object, which moves freely. The two cylindrical axes are paired in the alignment window of this tool, and the two spherical centers are paired. Once again, the alignment, if not perfect, is approximated to be as close as possible with the use of the least-squares algorithm.

Anatomical landmarks were virtually palpated on these 3D models using Geomagic Control for both manual and automatic methods. Data points were exported in the Initial Graphics Exchange Specification (IGES) file format, and were imported into MATLAB R2023b for processing, statistical analysis, and plotting.

The 3D printing was conducted using electron beam melting, while for the control group, standard Ti6Al4V cup and pedestal implants manufactured by Adler, Berlin, Germany, were used.

### 2.1. Experimental Study

The same surgeon operated on all of the patients. The surgical procedure for custom partial pelvic replacement involves the precise removal of the tumor-affected bone parts, guided by patient-specific instrumentation according to precise pre-operative planning. The custom implant (Figure 3) is then secured using screws and a main stem, ensuring stability and functionality. In cases where the insertion of the main stem is challenging, an alternative fixation approach using cortical screws is employed. The overall goal is to successfully replace the affected portion of the pelvis while maintaining structural symmetry with the contra-lateral healthy side.

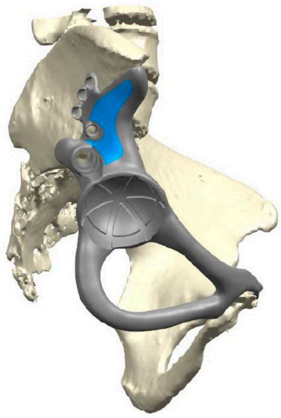

**Figure 3.** Positioned 3D-printed custom implant.

### 2.2. Anatomical Landmark Identification

Individual bones pertaining to each patient were imported as Standard Triangle Language (.stl) files into Geomagic Control, a program that allows for the detailed analysis of 3D models in a multi-purpose digital workspace. Once that is performed, virtual palpation of several anatomical landmarks is carried out. This was conducted in two ways: manual palpation and automatic palpation.

Manual palpation was used for anatomical landmarks on the sacrum, pelvic girdle, and the femur head. The sacral spine and both articular facets were palpated on the sacrum. However, due to excess noise in some scans, the sacral spine, along with both sacral alae, were identified as an alternative. For the anatomical reference frame construction, palpation of the anterior superior iliac spines, as well as the posterior superior iliac spines, was carried out as per the recommendations by the International Society of Biomechanics (ISB) [61]. These recommendations are based on a bone-embedded reference frame [62]. The greater trochanter is virtually palpated on the femur and is identified as the apex of the greater trochanter. Finally, for the acetabular inclination angle, a series of no less than 30 points were virtually palpated along each acetabular ridge. Automatic palpation for the femur heads' center was carried out using the best-fit sphere.

All of the coordinates of the palpated landmarks above were individually exported in the IGES format, which is used to store and exchange 3D-model data.

### 2.3. Post-Operation Morphological Parameter Measurement

Custom created MATLAB scripts were used to analyze the palpated landmarks, following a workflow divided into sections. Initially, anatomical reference frames were constructed according to ISB standards [61]. Mirroring the healthy pelvis landmarks about the healthy sacrum allowed for the creation of a complete set of landmarks for constructing a simulated healthy pre-operation reference frame of the entire pelvis. Hip joint center of rotation positions and their deviations from the contra-lateral side were calculated. Greater trochanter offset deviations were measured by comparing the greater trochanter offsets of the healthy and affected sides of each pelvis. Lastly, an acetabular inclination analysis involved fitting a plane onto a set of manually palpated ridge points and then measuring the inclination angle between its normal vector projected on the frontal plane and the vertical axis of the pelvis reference frame.

#### 2.3.1. Mirroring

Mirroring the health of the affected hemi-pelvis was performed using spatial registration using the sacrum of each individual patient as the mirroring plane (Figure 4). This process of mirroring the pelvis in the presence of imaging noise due to metal implants has been established as a viable method [63]. Mirroring is based on the bilateral symmetry of the pelvis [64]. Additionally, this process holds, given the fact that patients were selected with tumors in the region of P2. This means that tumor growth and surgical interventions occur away from the sacrum, which is used to construct the symmetry plane for the patient. This is unlike cases where tumor growth occurs in P4, which is on the sacrum. Such cases would compromise the anatomical landmarks on the sacrum, and thus would demand alternatives in unaffected regions.

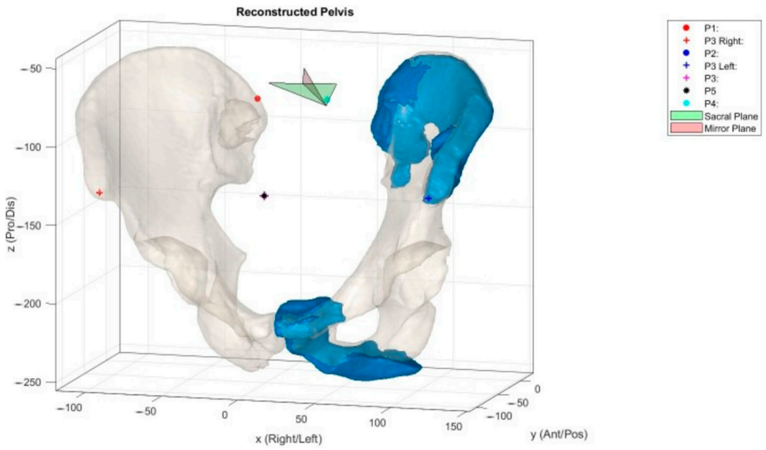


**Figure 4.** Simulated healthy pelvis (white) obtained by mirroring the healthy pelvis along the symmetry plane and the reconstructed pelvis (blue).

### 2.3.2. Simulated Healthy Pelvis Reference Frame

The palpated anatomical landmarks from the mirrored healthy pelvis underwent processing through a function that constructed the anatomical reference frame in alignment with ISB standards [62]. However, a 90 degree misalignment of the X and Y axes prompted the rotation of the reference frame about its Z axis. The result is the direction of the anatomical X, Y, and Z axes and the precise position of the reference frame origin. The direction of each axis was saved as a unit vector consisting of X, Y and Z coordinates in the global reference system. In addition, the global X, Y, and Z coordinates of the constructed reference frame origin were obtained.

### 2.3.3. Reference Frame Orientation and Positional Deviations

The reconstructed and healthy reference frames were imported (Figure 5), and the function used conformed with the established convention [65]. This quantified the orientation difference between the two. The origins' positions were compared, yielding angular and positional deviations, recorded on each axis of the healthy pelvis reference frame.

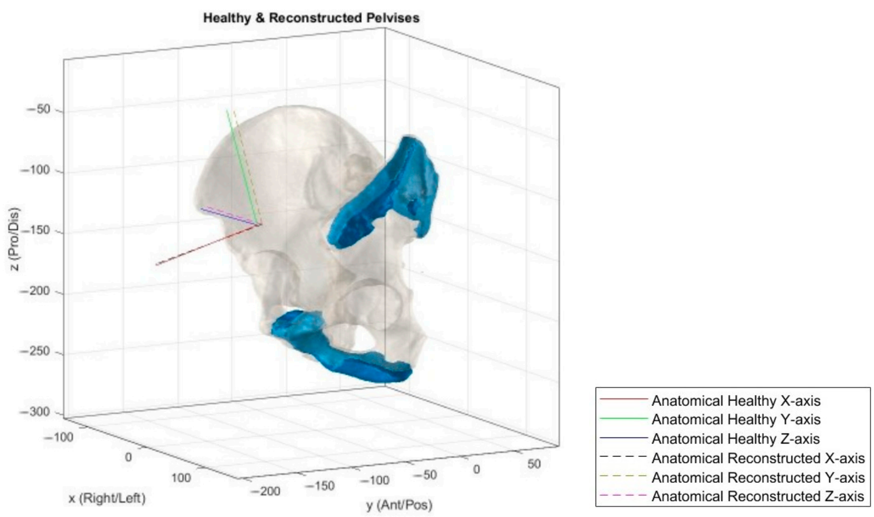


**Figure 5.** A superimposition of both reference frames based once on the reconstructed pelvis and once on the simulated healthy pelvis.

2.3.4. Centers of Rotation and Deviations

The reconstructed and healthy femoral head centers, representing rotation centers, alongside the healthy pelvis reference frame axes, were imported into MATLAB. The vector from each center to the reference frame origin was calculated by subtracting the anatomical reference frame origin vector from the hip center of the rotation vector. The resultant vector was then decomposed into each of the three axes of the pelvis reference frame. This was repeated for both the healthy and reconstructed hip center of rotations, and then the deviations were calculated.

2.3.5. Greater Trochanter Offset Deviations

Healthy pelvis reference frame axes were imported into MATLAB, along with both the reconstructed and healthy femoral head centers, as well as their corresponding greater trochanters. The vector for each hip center of rotation, as well as each greater trochanter apex, was obtained by comparing their positions with the anatomical reference frame origin. Then, these vectors were decomposed into each of the reference frame axes to obtain their local coordinates. Offset magnitudes of the reconstructed and healthy contra-lateral sides were calculated, as well as their deviations.

2.3.6. Acetabular Inclination Angle Analysis

A script by [66] was used to calculate the normal vector of the best-fit plane on the acetabular ridge (Figure 6). This vector was projected onto the pelvis reference frame's frontal plane, and the acetabular inclination angle was measured.

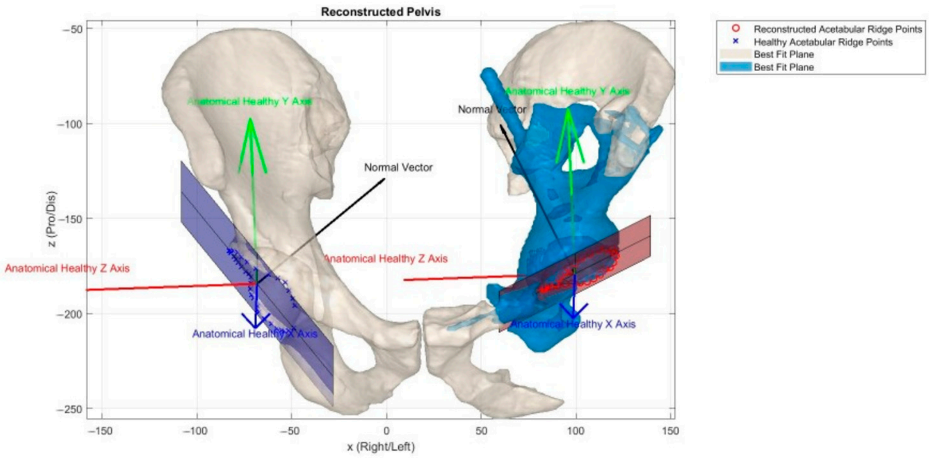


**Figure 6.** Best-fit planes along the acetabular ridges and their normal vectors.

First, the reconstructed inclination angle deviation was calculated by comparing it with the contra-lateral healthy side. Then, absolute reconstructed acetabular inclination angles were compared with the safe zones proposed in the literature [67,68], which have since been used as a convention, the former ranging from 30 to 50 degrees and the latter ranging from 30 to 45 degrees.

*2.4. Data Processing and Statistical Analysis*

All anatomical parameters are normalized based on the characteristic dimensions native to each personal hip. Those were based on the convention set by [69], which deems each of these dimensions to be representative of the overall pelvis size along each axis. In detail, parameters are reported in terms of mean ± standard deviation, along with observed minimum and maximum values when appropriate.

The variables, both measured and calculated, were all assessed using a Shapiro–Wilk test for normality. Normally distributed data were statistically analyzed using Student's *t*-test. However, the variances in each pair of data sets were first analyzed to determine if they had equal variances; this was performed using the two sample F-test. Non-normally distributed data were statistically analyzed using a non-parametric Mann–Whitney U-Test. Categorical data were analyzed using a Chi-squared test.

In all of the statistical analyses, a $p$-value of less than 0.05 was taken to reveal statistically significant differences; otherwise, non-significance was indicated.

An intra-observer reliability test was carried out by calculating the intra-class correlation coefficient (ICC) with a confidence interval of 95%. Four random patients were selected from each group, and an anatomical landmark used in the construction of the bone embedded anatomical reference frame was palpated a second time. The time between the first and second time landmark selections was no less than 6 weeks.

Calculations and graph productions were carried out using Matlab (Matlab®, R2022a, The MathWorks, Inc., Natick, MA, USA) and were supplemented with the use of Excel (Microsoft Corporation, Redmond, WA, USA) for preliminary analysis and data visualization.

Power Analysis

Power analyses were carried out at a power of 80% with a 0.05 probability confidence to select the proper patients' samples. A difference in terms of linear and rotational evaluations between the affected and contra-lateral healthy side within each group, as well as between the two groups, equal to 3 mm or degrees, both with a standard deviation of 2 mm or degrees, was hypothesized.

## 3. Results

### 3.1. Intra-Observer Reliability

For the eight patients selected across each of the three coordinates, r > 0.99. A more detailed breakdown of the ICC and the raw data are available in Appendix A.

### 3.2. Normalization Values

Following from the importance of considering the overall pelvic dimensions and how they may affect cross-comparisons, the intra-patient characteristic parameters used to normalize each of the three coordinates of the hip joint center of rotation were measured and are presented (Table 1).

**Table 1.** Geometrical parameters measured from each patient to be used for data normalization. All values are in millimeters.

| **Normalization Parameters** | | | | | | |
|---|---|---|---|---|---|---|
| | **3D-Printed Implant** | | | **Bone Graft** | | |
| Patient | Half Width | Depth | Height | Half Width | Depth | Height |
| 1 | 108.5 | 144.4 | 141.0 | 107.0 | 148.2 | 180.4 |
| 2 | 107.3 | 135.0 | 130.4 | 133.9 | 134.8 | 150.6 |
| 3 | 132.0 | 132.1 | 131.8 | 116.4 | 139.5 | 146.0 |
| 4 | 147.2 | 141.5 | 147.1 | 130.3 | 142.9 | 152.1 |
| 5 | 99.6 | 134.1 | 134.0 | 112.7 | 140.0 | 138.7 |
| 6 | 125.4 | 145.4 | 160.0 | 114.4 | 134.7 | 136.6 |
| 7 | 127.0 | 153.1 | 148.5 | 105.9 | 138.8 | 144.1 |
| 8 | 111.2 | 136.1 | 133.0 | 114.9 | 139.5 | 141.5 |

Pelvic depth measurements require only one side of the pelvis, which make the use of the healthy contra-lateral pelvis sufficient without the need for mirroring, as was performed with the pelvic width. This dimension, once averaged across all patients, was found to be 14.0 cm.

### 3.3. Hip Center of Rotation

This parameter is analyzed in two ways. Firstly, the absolute positions of the contra-lateral healthy and the reconstructed hip centers of rotation are compared within each group for an accuracy analysis. Secondly, the deviations of this parameter in the reconstructed side of the pelvis when compared to the healthy contra-lateral side of the pelvis are compared across groups for a precision analysis.

#### 3.3.1. Absolute Values of Hip Center of Rotation

A Student's *t*-test showed no significant difference, *p*-value > 0.05, between the positioning of the reconstructed hip center of rotation when compared to the healthy contra-lateral hip center of rotation on all three axes (Table 2) in both groups. This shows that there is accurate reconstruction of this parameter when using 3D-printed customized implants, as well as with manual bone graft reconstruction.

**Table 2.** Positions of the healthy as well as the reconstructed hip centers of rotation measured based on the anatomical reference frame of the simulated healthy pelvis. All values are in millimeters.

| | **Absolute Positions of Hip Center of Rotation** | | | | | | | | | | | |
|---|---|---|---|---|---|---|---|---|---|---|---|---|
| | **3D-Printed Implant** | | | | | | **Bone Graft** | | | | | |
| | Healthy | | | Reconstructed | | | Healthy | | | Reconstructed | | |
| | X | Y | Z | X | Y | Z | X | Y | Z | X | Y | Z |
| Max | −31.2 | −66.6 | 91.7 | −23.5 | −61.6 | 105.3 | −26.4 | −66.9 | 85.7 | −12.5 | −53.8 | 85.3 |
| Min | −45.8 | −88.4 | −93.6 | −50.3 | −95.9 | −91.3 | −43.0 | −86.7 | −87.9 | −47.0 | −92.9 | −89.9 |
| Median | −36.8 | −73.4 | 87.5 * | −32.1 | −71.2 | 85.2 * | −33.3 | −71.4 | 83.0 * | −33.8 | −71.5 | 80.9 * |
| Standard Deviation | 4.5 | 7.5 | 3.1 * | 9.7 | 11.7 | 8.5 * | 5.2 | 6.6 | 3.3 * | 10.0 | 13.2 | 6.4 * |

* For both the median and the standard deviation of the Z coordinate, only the magnitude was considered, given that the hip center of rotation for both the healthy and the reconstructed pelvises varies between sides from one patient to another.

#### 3.3.2. Deviations in Hip Center of Rotation

Across all axes and between both groups, the bone graft procedure has the greatest absolute deviation of 20.3 mm along the Inferior/Superior Y axis (Table 3). A Student's *t*-test was performed for the anterior/posterior position and the inferior/superior position, while a non-parametric Mann–Whitney-U test was used for the non-normally distributed medio/lateral position.

**Table 3.** The characteristic values of deviations in each reconstructed hip center of rotation. All values are in millimeters.

| | **Hip Center of Rotation Deviations** | | | | | |
|---|---|---|---|---|---|---|
| | **3D-Printed Implant** | | | **Bone Graft** | | |
| | X | Y | Z | X | Y | Z |
| Max | 8.1 | 9.1 | 16.7 | 15.1 | 18.6 | 3.3 |
| Min | −8.8 | −7.6 | −4.3 | −8.0 | −20.3 | −19.8 |
| Median | 5.0 | −1.4 | 4.0 | 0.3 | −0.4 | −0.7 |
| Standard Deviation | 6.7 | 5.3 | 5.9c | 6.8 | 13.1 | 7.1 |

Note: There is an agreement in the literature that the optimal reconstruction deviation for the hip center of rotation is ±5 mm [70,71].

### 3.4. Greater Trochanter Offset

This parameter is analyzed in two ways, discussed below.

#### 3.4.1. Absolute Offset

Firstly, the absolute offsets of the contra-lateral healthy and the reconstructed greater trochanters were compared within each group for an accuracy analysis. Representative values were extracted (Table 4). A Student's *t*-test showed no significant difference, *p*-value > 0.05, in absolute values of the healthy compared to the reconstructed parameters within each group.

**Table 4.** The characteristic values of the greater trochanter offset magnitudes. All values are in millimeters.

| | Greater Trochanter Offset Magnitudes | | | |
|---|---|---|---|---|
| | **3D-Printed Implant** | | **Bone Graft** | |
| | Healthy | Reconstructed | Healthy | Reconstructed |
| Max | 51.0 | 59.2 | 58.5 | 57.7 |
| Min | 40.4 | 42.1 | 42.2 | 37.0 |
| Median | 44.2 | 46.7 | 48.6 | 48.7 |
| Standard Deviation | 44.5 | 49.1 | 49.4 | 48.5 |

#### 3.4.2. Offset Deviations

Secondly, the deviations of this parameter in the reconstructed side of the pelvis when compared to the healthy contra lateral side were compared across groups for a precision analysis. Representative values were extracted (Table 5). The greater trochanter offset deviations showed no significant difference, *p*-value < 0.05, between both groups.

**Table 5.** Characteristic values of the greater trochanter offset deviations. All values are in millimeters.

| | Greater Trochanter Offset Deviation | |
|---|---|---|
| | **3D-Printed Implant** | **Bone Graft** |
| Max | 15.7 | 10.4 |
| Min | −1.0 | −11.1 |
| Median | 2.6 | −0.4 |
| Standard Deviation | 5.5 | 6.6 |

### *3.5. Acetabular Inclination Angles*

This parameter was analyzed in two ways, discussed below.

#### 3.5.1. Inclination Angles

First, the representative values of the acetabular inclination angles were extracted (Table 6).

**Table 6.** Characteristic values of the acetabular inclination angles in degrees.

| | Acetabular Inclination Angles | | | |
|---|---|---|---|---|
| | **3D-Printed Implant** | | **Bone Graft** | |
| | Reconstructed | Healthy | Reconstructed | Healthy |
| Max | 61.4 | 63.5 | 48.8 | 61.1 |
| Min | 42.9 | 51.9 | 15.3 | 50.2 |
| Median | 50.1 | 56.0 | 32.5 | 55.3 |
| Standard Deviation | 6.3 | 4.0 | 9.5 | 3.4 |

Note: there are two conventional safe zones [67,68], the former ranges from 30 to 50 degrees and the latter from 30 to 45 degrees.

The acetabular inclination angle was assessed using a Chi-squared test. This was performed twice, each time considering the different one of the two safe zones in (Figure 7), both with a null hypothesis being that there is no difference between both methods at an alpha level of 0.05. No significant difference was found between both groups in all cases.

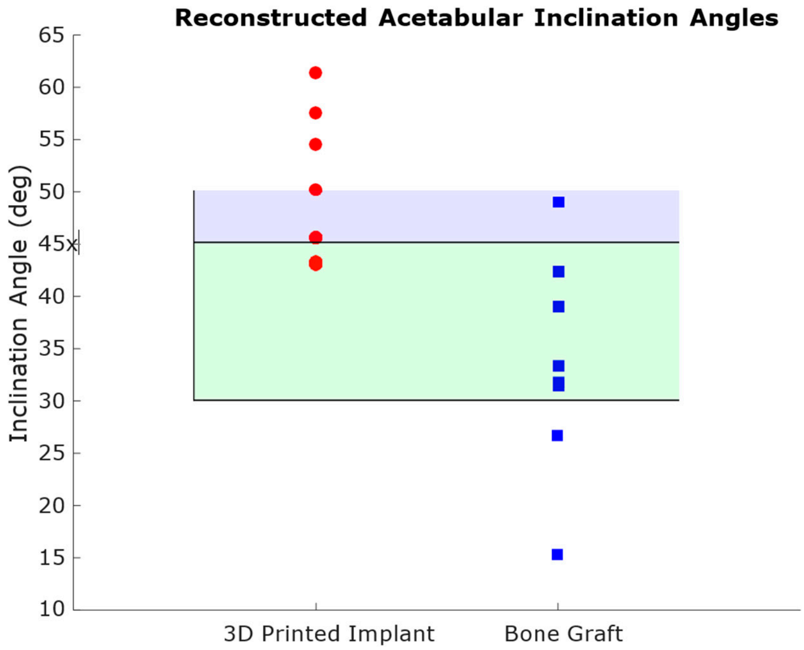


**Figure 7.** Acetabular inclination angles superimposed on relevant safe zones. (Note: the green zone represents the [67] safe zone, and the green + blue zones together represent the [68] safe zone).

### 3.5.2. Deviations in Inclination Angles

Secondly, the deviations were calculated relative to the contra-lateral healthy inclination angle projected onto the reconstructed side of the pelvis, characteristic values were extracted in (Table 7). A Student's $t$-test was carried out on the deviation data and yielded a significant difference, $p$-value $< 0.001$, between both groups. It was found that the 3D-printed implant group had a deviation significantly closer to 0 than the bone graft group.

**Table 7.** Characteristic values of the acetabular inclination angle deviations. All measurements are in degrees.

| | Acetabular Inclination Angle Deviation | |
|---|---|---|
| | **3D Printed** | **Bone Graft** |
| Max | 6.2 | −7.9 |
| Min | −18.1 | −38.6 |
| Median | −4.8 | −21.2 |
| Standard Deviation | 7.6 | 10.5 |

## 4. Discussion

This project spanned more than one technological advancement and encompassed thorough analyses to verify and validate the efficacy of their practical implementations. All of the results show integrity in precision through intra-observer repeatability tests, which show excellent ICC and accuracy through cross-referencing established values in the literature. Importantly, the procedure using 3D-printed custom implants was compared with a conventional approach that uses bone grafts and standard off-the-shelf implants, both of which, in this study, were homogenized in terms of patient demographics and surgical procedure of the tumor resection. Given the detailed and meticulous nature of the analyses, each parameter is discussed at a high level. However, in general, it has been found that all measures of precision and accuracy were statistically comparable, except that the precision of reconstruction of the acetabular inclination angle of the 3D-printed implant group was higher. Given the fact that all 16 patients were operated on by the same experienced senior surgeon, these results are favorable for the advocacy of using 3D-printed customized implants to guarantee a consistently high standard of skeletal surgical reconstruction, especially as a preventative measure of error with less-experienced surgeons and a comforting factor for patients. While the focus of this study is on the impact that 3D-printed personalized implants have intra-operatively, the improved reconstruction can explain the reported survival rates of custom 3D-printed implants from three studies, two at approximately 3 years follow-up [22,23] and one at 5 years follow-up [10]. The survival rates of the 3D-printed personalized implants were found to be acceptable.

### 4.1. Reference Frame and Pelvis Size

To ensure the validity of the findings, the first consideration is whether or not the methods of data acquisition and analysis are reliable. The three pelvic dimensions, width, depth, and height, which were used for data normalization, are within range of those reported in the literature. The calculated average pelvis width of all 16 patients in this report is 23.7 cm, while in the literature it is reported as 23.8 cm [69]. The calculated average depth in this report is 14.0 cm, while that in the literature is 16.4 cm [69]. It is worth noting that that that study involved a larger population, 65, compared to this study, having 16.

Given the variation in individual pelvises due to several factors such as sex, height, and ethnicity, as well as due to differences in sample sizes, the differences between present measured dimensions and those found in the literature are expected. As such, the need for data normalization based on individual pelvis size was vital.

This affirmation covers several technical points of the methodology. Firstly, the 3D reconstruction of the 2D CT medical images taken post-operatively was performed without critical loss of bone boundaries; thus, the preservation of anatomical landmarks is guaranteed. Secondly, the location and orientation of each of the five bones present within every pelvis were consistent throughout the process, which involved various procedures and spanned three different software. Thirdly, the manual palpation of anatomical landmarks for the reference frame creation, as well as the critical parameters selection, is reliable. Fourthly, the decision to simulate a healthy pelvis that is pre-operative and tumor free was correct, and the method used to create a mirroring plane is also correct [72]. Fifthly, the custom written code for the morphological analysis is error free.

All further analyses yielded results with greater confidence, given these confirmations.

### 4.2. Hip Center of Rotation

There is great importance in the symmetry between both sides of the pelvis for the best functional and clinical outcomes. This is why the statistically accurate reconstruction of the hip center of rotation in the 3D-printed customized implant group is a desirable result [37]. Its degree of error is the main impacting factor of, and is directly proportional to, the decrease in the range of motion. There is also an influence from the hip center of rotation on the range of motion [38], and, in addition, a tendency of decreased range of motion based on the type of anterior inferior iliac spine anatomy post-reconstruction [73]. This further compounds the demands on the surgeon during manual reconstruction when using a bone graft. However, such an anatomical requirement can be simply incorporated into the 3D-printed implant during the design stage and not worried about during the surgery.

Following from that, the positions of the reconstructed hip center of rotation were not found to be significantly different in both groups, $p$-value > 0.05, from the target position.

Additionally, the precision of the reconstruction was found to be not significantly different, $p$-value > 0.05, between both groups. This suggests that the imaging procedure, design software, and 3D-printing equipment can guarantee small errors, as an experienced surgeon would have in a manual procedure. The production workflow has proven to be consistent and reliable; thus, it increases confidence in this approach. Especially with the complex geometry of the pelvis, as well as other bones in the body where restricted access might prevent sufficient recreation of the native anatomy, pre-printed implants can circumvent this issue. As a result, and as already seen in the literature, surgical time is decreased significantly [74]. This trend of reduced surgical time has also been observed with the use of 3D-printed anatomical models for training and planning [75,76].

### 4.3. Greater Trochanter Offset

The mean distance measured from the greater trochanter to the femur head center for the healthy side of the pelvis across all 16 patients is 48.8 mm, while that on the reconstructed side is 47.0 mm. A study on 293 subjects, using 3D analysis tools, obtained an average distance from the greater trochanter to the femur head center of 46.8 $\pm$ 4.3 mm [40]. This increases confidence in the data acquisition method as well as the data processing procedure. Given that the greater trochanter offset also includes the position of the primary parameter, i.e., the hip center position, it can be concluded that both manual palpation, as well as the best-fit methods of target identification, are accurate.

The reconstructed greater trochanter offsets using the 3D-printed implants and the conventional method were not found to be significantly different from their healthy contra-lateral comparisons. This signifies another major advantage for this proposed procedure, as orthopedic surgeons are always looking for better ways to restore the femur head center, and the greater trochanter has been identified as a suitable parameter for it [40]. In addition, the deviation in reconstruction of the greater trochanter using the 3D-printed implant is statistically comparable to the deviation by the conventional bone graft and standard-sized off-the-shelf implant replacement. This high degree of precision is a strong indicator of superior post-operative outcomes [77–79].

### 4.4. Acetabular Inclination Angle

While the previous parameters showed comparable results between the two surgical methods, a key difference emerged in the analysis of the acetabular inclination angle. The deviation in the reconstructed acetabular inclination angle was the only one to present a significant difference, where the 3D-printed implant group had a more superior precision, $p$-value $< 0.001$. This is a clear indication of the advantages that 3D-printed customized implants have, because a more precisely reconstructed inclination angle reduces the risk of impingement of the femur implant neck with the acetabulum implant cup and subsequent dislocation by increasing the range of motion [53,80,81], which directly increases the prosthesis survivorship. Even with the presence of an experienced surgeon that has carried out a high volume of massive hip replacements, there is still room for improvement.

With the use of 3D-printed personalized implants, patient-specific instrumentation can also be produced to better execute the planned tumor resection process intra-operatively. This is as a result of having already recreated the 3D model of the patient anatomy. Additionally, the personalized implant better mimics the native patient anatomy compared to standard off-the-shelf implants. Both factors can contribute to superior precision in reconstructing the acetabular inclination angle.

Some reconstructed acetabular inclination angles are intentionally outside both safe zones due to the fact that not every patient will benefit from being in the average range of angles [82,83], especially in this case, where the angle was chosen by the surgeons during pre-operative planning to match the healthy contra-lateral inclination angle.

### 4.5. Limitations and Suggestions for Further Work

The pelvic bone is a complex structure and a pivotal one; it acts as the stress-bearing unit in the body and is central to various movements. That is why there is a plethora of features that could be analyzed for reconstruction success. So far, the parameters analyzed were chosen for their direct impacts on critical functional outcomes. Through discussions with expert orthopedic surgeons and biomedical engineering scientists, it was concluded that a supplementary parameter, the pelvic ring continuity, identified for its stress-distribution influence [25], would provide additional insight into the surgical outcomes. Given the static and dynamic forces acting on the pelvis, an ideal reconstruction would ensure a shape that uniformly distributes the generated stress and shear. Otherwise, incomplete pelvic ring reconstruction may lead to degeneration of the sacroiliac joint or endoprosthetic breakage [84,85]. That is why, in the future, more understanding of the biomechanics of the pelvis under daily living activities will be exploited for improved custom 3D-printed implant design [86]. From the theoretical and technical knowledge gleaned from this work, a proposed method for analysis is a distance map analysis. Since the healthy pelvis anatomy is shaped for ideal stress distribution, measuring the superimposition of the reconstructed bones from both procedures would give a strong indication of which is better.

The number of patients involved was sufficient to yield statistical significance. To further uncover the advantages of 3D-printed customized implants, a bigger cohort would suffice, given that other aspects of this study are satisfactory.

Every aspect of both surgical procedures were uniform to limit the impacting factors. This comparison, with the presence of an expert surgeon, provided clear evidence that 3D-printed customized implants can match the output level of a senior surgeon. It would thus follow to conduct this comparison with a junior surgeon to understand whether the accuracy and precision of the 3D-printed customized implant is dependent on the expertise of a senior surgeon during its placement.

Additionally, the customizable nature of 3D-printed designs means that there are various patterns and textures that are available. An important part of implant success is the integration of the implant material with the hosting bone. Thus, it would prove insightful to analyze the most effective surface designs in avoiding foreign body rejection.

In the future, bio-printing can be incorporated and tested with this procedure to investigate the possibility of promoting the repair process of the reconstructed bone [87,88] by pre-printing the implant with bio-inks containing growth factors, cells, and bio-materials.

## 5. Conclusions

In this study, the impact of using customized 3D-printed hip implants on massive pelvic reconstruction has been investigated in comparison to the conventional use of bone grafts and standard-sized off-the-shelf implants. The morphological impact of both procedures was assessed through a custom workflow for data acquisition and processing involving three key parameters: hip joint center of rotation, greater trochanter offset, and acetabular inclination angle. The accuracy and precision of each parameter were assessed and compared between both procedures.

Firstly, this study successfully developed and validated a reliable workflow for data acquisition and processing, from medical image segmentation to morphological parameter analysis, as evidenced by the high intra-observer reliability (ICC > 0.99) across all of the measured coordinates. The calculated average hip width and depth of all 16 patients in this report are 23.7 cm and 14.0 cm, respectively, while [69] reported 23.8 cm and 16.4 cm, respectively. Given the variation in individual pelvises due to several factors such as sex and ethnicity, as well as due to differences in sample sizes, differences between the measured dimensions and those found in the literature are expected.

Secondly, 3D-printed custom implants demonstrated the ability to accurately reconstruct the hip joint center of rotation, greater trochanter offset, and acetabular inclination angle ($p > 0.05$ for all three), comparable to the conventional bone graft with the standard-sized off-the-shelf implant method.

Thirdly, 3D-printed implants exhibited superior precision in reconstructing the acetabular inclination angle, with a significantly lower median deviation of $-4.8$ degrees compared to $-21.2$ degrees for bone grafts ($p < 0.001$), indicating potential for improved post-operative outcomes.

In this study, three morphological parameters were measured to compare the use of personalized 3D-printed implants with standard-sized off-the-shelf implants in pelvic reconstruction. The custom 3D-printed implants showed statistically significant improvements in the precision of reconstructing the acetabular inclination angle. This supports the use of 3D-printed custom implants in complex hip reconstructions, which goes in line with the trend of incorporating 3D printing in various applications within healthcare. This shows the potential for this technology to become the standard of care in complex hip reconstructions, especially in cases involving massive bone loss. This study found statistical significance in the study population. However, in future studies, a larger patient sample could elucidate further differences between both procedures to give an even more in-depth understanding of the impact custom 3D-printed implants have on reconstruction surgeries. Additionally, given the customizable nature of 3D printing materials, bio-printing with the use of bioactive materials could be introduced to try to reduce the risk of implant rejection and improve osseointegration.

**Author Contributions:** Conceptualization, D.M.D., A.L., C.B. and B.S.; methodology, C.B. and Y.H.; software, C.B. and Y.H.; validation, C.B. and Y.H.; formal analysis, C.B. and Y.H.; investigation, C.B. and Y.H.; resources, D.M.D., A.L., C.B. and B.S.; data curation, C.B. and Y.H.; writing—original draft preparation, Y.H.; writing—review and editing, A.L., C.B. and Y.H.; visualization, C.B. and Y.H.; supervision, A.L., B.S. and C.B.; project administration, C.B. and A.L.; funding acquisition, not applicable. All authors have read and agreed to the published version of the manuscript.

**Funding:** This study was partially funded by the Italian Ministry of Health under the "5 per mille" program.

**Institutional Review Board Statement:** This study was conducted in accordance with the Declaration of Helsinki and was approved by the Ethics Committee (Prot. Gen. 0008191 on 27 May 2021) of the IRCCS Istituto Ortopedico, Bologna-Italy (Cod. CE AVEC: EM468/2021_47/2014/Oss/IOR_EM1).

**Informed Consent Statement:** Informed consent was obtained from all subjects involved in this study.

**Data Availability Statement:** Data are available from the corresponding authors upon reasonable request.

**Conflicts of Interest:** The authors declare no conflicts of interest.

## Abbreviations

The following abbreviations are used in this manuscript:

| | |
|---|---|
| 3D | Three-dimensional |
| CT | Computed Tomography |
| IQR | Inter-quartile range |
| ISO | International Organization for Standardization |
| STL | Standard triangle language |
| IGES | Initial Graphics Exchange Specification |
| CSV | Comma-separated values |

## Appendix A

*Intra-Observer Reliability*

The raw data (Tables A1 and A2) represent the global coordinates of the anatomical landmark, which is why there will be no match with any of the other reported coordinates that are based on the locally constructed bone-embedded reference frame. The reason global data were chosen for this reliability analysis is because they constitute the foundation on which all other values are acquired. By establishing the reliability in these palpations, all other manual palpations are similarly validated.

ICC calculations were based on the formula by [89], using the corresponding MATLAB script written by Arash Salarian [90].

**Table A1.** Raw data of anatomical landmark coordinates from the 3D-printed implant group used for intra-observer reliability analysis.

| | 3D-Printed Implant | | | | | |
|---|---|---|---|---|---|---|
| **Random Patient Number** | **Anatomical Landmark Palpations** | | | | | |
| | X1 (mm) | X2 (mm) | Y1 (mm) | Y2 (mm) | Z1 (mm) | Z2 (mm) |
| 1 | −79.7 | −78.5 | 192.7 | 192.1 | −83.7 | −83.2 |
| 2 | −67.7 | −68.6 | 223.4 | 223.6 | −317.7 | −318.0 |
| 3 | 39.7 | 38.6 | 200.4 | 200.9 | −171.7 | −175.6 |
| 4 | 56.7 | 55.8 | 110.5 | 109.5 | −25.0 | −24.4 |
| r | 0.99 | 0.99 | 0.99 | 0.99 | 0.99 | 0.99 |

**Table A2.** Raw data of anatomical landmark coordinates from the bone graft group used for intra-observer reliability analysis.

| | Bone Graft | | | | | |
|---|---|---|---|---|---|---|
| **Random Patient Number** | **Anatomical Landmark Palpations** | | | | | |
| | X1 (mm) | X2 (mm) | Y1 (mm) | Y2 (mm) | Z1 (mm) | Z2 (mm) |
| 1 | −30.8 | −29.7 | 66.2 | 67.2 | −109.9 | −113.4 |
| 2 | 41.9 | 36.7 | 88.3 | 88.7 | −112.5 | −121.0 |
| 3 | 39.6 | 38.5 | −49.9 | −50.9 | −1156.8 | −1157.5 |
| 4 | 51.9 | 53.3 | 99.2 | 100.0 | −18.4 | −18.6 |
| r | 0.99 | 0.99 | 0.99 | 0.99 | 0.99 | 0.99 |

## References


1. Hellman, S.; Frisch, P.; Platzman, A.; Booth, P. 3D Printing in a hospital: Centralized clinical implementation and applications for comprehensive care. *Digit. Health* **2023**, *9*, 20552076231221899. [CrossRef] [PubMed]
2. Kumar Gupta, D.; Ali, M.H.; Ali, A.; Jain, P.; Anwer, M.K.; Iqbal, Z.; Mirza, M.A. 3D printing technology in healthcare: Applications, regulatory understanding, IP repository and clinical trial status. *J. Drug Target.* **2022**, *30*, 131–150. [CrossRef] [PubMed]
3. Dodziuk, H. Applications of 3D printing in healthcare. *Kardiochirurgia I Torakochirurgia Pol. Pol. J. Thorac. Cardiovasc. Surg.* **2016**, *13*, 283–293. [CrossRef] [PubMed]
4. Andreadis, I.I.; Gioumouxouzis, C.I.; Eleftheriadis, G.K.; Fatouros, D.G. The Advent of a New Era in Digital Healthcare: A Role for 3D Printing Technologies in Drug Manufacturing? *Pharmaceutics* **2022**, *14*, 609. [CrossRef]
5. Woo, S.H.; Sung, M.J.; Park, K.S.; Yoon, T.R. Three-dimensional-printing Technology in Hip and Pelvic Surgery: Current Landscape. *Hip Pelvis* **2020**, *32*, 1–10. [CrossRef]
6. Tasneem, I.; Ariz, A.; Bharti, D.; Haleem, A.; Javaid, M.; Bahl, S. 3D Printing Technology and its Significant Applications in the Context of Healthcare Education. *J. Ind. Integr. Manag.* **2023**, *8*, 113–130. [CrossRef]
7. Fadero, P.E.; Shah, M. Three dimensional (3D) modelling and surgical planning in trauma and orthopaedics. *Surg.* **2014**, *12*, 328–333. [CrossRef]
8. Tack, P.; Victor, J.; Gemmel, P.; Annemans, L. 3D-printing techniques in a medical setting: A systematic literature review. *Biomed. Eng. Online* **2016**, *15*, 115. [CrossRef]
9. Di Laura, A.; Henckel, J.; Hart, A. Custom 3D-Printed Implants for Acetabular Reconstruction: Intermediate-Term Functional and Radiographic Results. *JBJS Open Access* **2023**, *8*, e22. [CrossRef]
10. Zoccali, C.; Baldi, J.; Attala, D.; Scotto di Uccio, A.; Cannavò, L.; Scotto, G.; Luzzati, A. 3D-Printed Titanium Custom-Made Prostheses in Reconstruction after Pelvic Tumor Resection: Indications and Results in a Series of 14 Patients at 42 Months of Average Follow-Up. *J. Clin. Med.* **2021**, *10*, 3539. [CrossRef]
11. Donati, D.; Di Liddo, M.; Zavatta, M.; Manfrini, M.; Bacci, G.; Picci, P.; Capanna, R.; Mercuri, M. Massive bone allograft reconstruction in high-grade osteosarcoma. *Clin. Orthop. Relat. Res.* **2000**, *377*, 186–194. [CrossRef] [PubMed]
12. Gebhardt, M.C.; Flugstad, D.I.; Springfield, D.S.; Mankin, H.J. The use of bone allografts for limb salvage in high-grade extremity osteosarcoma. *Clin. Orthop. Relat. Res.* **1991**, *270*, 181–196. [CrossRef]
13. Delloye, C.; Banse, X.; Brichard, B.; Docquier, P.L.; Cornu, O. Pelvic reconstruction with a structural pelvic allograft after resection of a malignant bone tumor. *J. Bone Jt. Surgery. Am. Vol.* **2007**, *89*, 579–587. [CrossRef]

14. Fujiwara, T.; Ogura, K.; Christ, A.; Bartelstein, M.; Kenan, S.; Fabbri, N.; Healey, J. Periacetabular reconstruction following limb-salvage surgery for pelvic sarcomas. *J. Bone Oncol.* **2021**, *31*, 100396. [CrossRef] [PubMed]
15. Ozaki, T.; Hillmann, A.; Bettin, D.; Wuisman, P.; Winkelmann, W. High complication rates with pelvic allografts. Experience of 22 sarcoma resections. *Acta Orthop. Scand.* **1996**, *67*, 333–338. [CrossRef]
16. Sohn, H.S.; Oh, J.K. Review of bone graft and bone substitutes with an emphasis on fracture surgeries. *Biomater. Res.* **2019**, *23*, 9. [CrossRef]
17. Jansen, J.A.; van de Sande, M.A.J.; Dijkstra, P.D.S. Poor long-term clinical results of saddle prosthesis after resection of periacetabular tumors. *Clin. Orthop. Relat. Res.* **2013**, *471*, 324–331. [CrossRef]
18. Danisman, M.; Mermerkaya, M.U.; Bekmez, S.; Ayvaz, M.; Atilla, B.; Tokgozoglu, A.M. Reconstruction of periacetabular tumours with saddle prosthesis or custom-made prosthesis, functional results and complications. *Hip Int. J. Clin. Exp. Res. Hip Pathol. Ther.* **2016**, *26*, 14–18. [CrossRef]
19. Fuchs, B.; O'Connor, M.I.; Kaufman, K.R.; Padgett, D.J.; Sim, F.H. Iliofemoral arthrodesis and pseudarthrosis: A long-term functional outcome evaluation. *Clin. Orthop. Relat. Res.* **2002**, *397*, 29–35. [CrossRef]
20. Li, C.; Wang, L.; Perka, C.; Trampuz, A. Clinical application of robotic orthopedic surgery: A bibliometric study. *BMC Musculoskelet. Disord.* **2021**, *22*, 968. [CrossRef]
21. Wong, K.C.; Kumta, S.M. Use of Computer Navigation in Orthopedic Oncology. *Curr. Surg. Rep.* **2014**, *2*, 47. [CrossRef] [PubMed]
22. Broekhuis, D.; Boyle, R.; Karunaratne, S.; Chua, A.; Stalley, P. Custom designed and 3D-printed titanium pelvic implants for acetabular reconstruction after tumour resection. *HIP Int.* **2023**, *33*, 905–915. [CrossRef] [PubMed]
23. Sun, W.; Li, J.; Li, Q.; Li, G.; Cai, Z. Clinical effectiveness of hemipelvic reconstruction using computer-aided custom-made prostheses after resection of malignant pelvic tumors. *J. Arthroplast.* **2011**, *26*, 1508–1513. [CrossRef] [PubMed]
24. Nieminen, J.; Pakarinen, T.K.; Nieminen, J. OrthOpaedic recOnstructiOn of cOmplex pelvic bOne defects. evaluatiOn Of variOus treatment methods. *Scand. J. Surg.* **2013**, *102*, 36–41. [CrossRef] [PubMed]
25. Hu, X.; Lu, M.; Zhang, Y.; Li, Z.; Wang, J.; Wang, Y.; Xing, Z.; Yang, X.; Tu, C.; Min, L. Pelvic-girdle reconstruction with three-dimensional-printed endoprostheses after limb-salvage surgery for pelvic sarcomas: Current landscape. *Br. J. Surg.* **2023**, *110*, 1712–1722. [CrossRef]
26. Zanchini, F.; Piscopo, A.; Cipolloni, V.; Vitiello, R.; Piscopo, D.; Fusini, F.; Cacciapuoti, S.; Panni, A.S.; Pola, E. The major proximal femoral defects: Megaprosthesis in non oncological patients-A case series. *Orthop. Rev.* **2023**, *15*, 38432. [CrossRef]
27. Grimer, R.J.; Carter, S.R.; Tillman, R.M. Allograft reconstruction of the acetabulum after resection of stage-IIB sarcoma. Intermediate-term results. *J. Bone Jt. Surgery. Am. Vol.* **1998**, *80*, 1396–1397. [CrossRef]
28. Langlais, F.; Lambotte, J.C.; Thomazeau, H. Long-Term Results of Hemipelvis Reconstruction with Allografts. *Clin. Orthop. Relat. Res.* **2001**, *388*, 178–186. [CrossRef]
29. Yoshida, Y.; Osaka, S.; Mankin, H.J. Hemipelvic allograft reconstruction after periacetabular bone tumor resection. *J. Orthop. Sci. Off. J. Jpn. Orthop. Assoc.* **2000**, *5*, 198–204. [CrossRef]
30. Beadel, G.P.; McLaughlin, C.E.; Wunder, J.S.; Griffin, A.M.; Ferguson, P.C.; Bell, R.S. Outcome in two groups of patients with allograft-prosthetic reconstruction of pelvic tumor defects. *Clin. Orthop. Relat. Res.* **2005**, *438*, 30–35. [CrossRef]
31. Hillmann, A.; Hoffmann, C.; Gosheger, G.; Rödl, R.; Winkelmann, W.; Ozaki, T. Tumors of the pelvis: Complications after reconstruction. *Arch. Orthop. Trauma Surg.* **2003**, *123*, 340–344. [CrossRef] [PubMed]
32. Fiore, M.; Paolucci, A.; Zunarelli, R.; Bortoli, M.; Montanari, A.; Pace, A.; Di Prinzio, L.; Parisi, S.C.; De Cristofaro, R.; De Paolis, M.; et al. A Combined Use of Custom-Made Partial Pelvic Replacement and Proximal Femur Megaprosthesis in the Treatment of Severe Bone Loss after Multiple Total Hip Arthroplasty Revisions. *Prosthesis* **2023**, *5*, 1093–1110. [CrossRef]
33. Moore, K.D.; McClenny, M.D.; Wills, B.W. Custom triflange acetabular components for large acetabular defects: Minimum 10-year follow-up. *Orthopedics* **2018**, *41*, E316–E320. [CrossRef] [PubMed]
34. Valente, G.; Benedetti, M.G.; Paolis, M.D.; Sambri, A.; Frisoni, T.; Leardini, A.; Donati, D.M.; Taddei, F. Long-term functional recovery in patients with custom-made 3D-printed anatomical pelvic prostheses following bone tumor excision. *Gait Posture* **2022**, *97*, 73–79. [CrossRef]
35. Hu, X.; Chen, Y.; Cai, W.; Cheng, M.; Yan, W.; Huang, W. Computer-Aided Design and 3D Printing of Hemipelvic Endoprosthesis for Personalized Limb-Salvage Reconstruction after Periacetabular Tumor Resection. *Bioengineering* **2022**, *9*, 400. [CrossRef]
36. Bruschi, A.; Cevolani, L.; Spazzoli, B.; Focaccia, M.; Pasini, S.; Frisoni, T.; Donati, D.M. Periacetabular Tumour Resection under Anterosuperior Iliac Spine Allows Better Alloprosthetic Reconstruction than Above: Bone Contact Matters. *J. Clin. Med.* **2022**, *11*, 4499. [CrossRef]
37. Hu, Y.; Zou, D.; Sun, Q.; Jiang, M.; Li, H.; Tsai, T.Y.; Zhang, J. Postoperative Hip Center Position Associated with the Range of Internal Rotation and Extension During Gait in Hip Dysplasia Patients After Total Hip Arthroplasty. *Front. Bioeng. Biotechnol.* **2022**, *10*, 831647. [CrossRef]
38. Tabata, T.; Kaku, N.; Tagomori, H.; Tsumura, H. Influence of hip center position, anterior inferior iliac spine morphology, and ball head diameter on range of motion in total hip arthroplasty. *Orthop. Traumatol. Surg. Res.* **2019**, *105*, 23–28. [CrossRef]
39. Luo, Y.; Sheng, H.; Zhou, Y.; Min, L.; Tu, C.; Luo, Y. Modular Hemipelvic Prosthesis Preserves Normal Biomechanics and Showed Good Compatibility: A Finite Element Analysis. *J. Funct. Biomater.* **2024**, *15*, 276. [CrossRef]

40. Tian, Z.; Mao, X.; Gao, Z.; Chen, B.; Wang, Z.; Yin, Z.; Guo, Z.; Gao, Z.; Xiang, C. A simple method for restoring the femoral head center in hip arthroplasty: A 3-dimensional analysis in the Chinese population. *BMC Musculoskelet. Disord.* **2022**, *23*, 986. [CrossRef]
41. Zaghloul, A. Hip Joint: Embryology, Anatomy and Biomechanics. *Biomed. J. Sci. Tech. Res.* **2018**, *12*. [CrossRef]
42. Harty, M. The Anatomy of the Hip Joint. In *Surgery of the Hip Joint: Volume 1*; Tronzo, R.G., Ed.; Springer New York: New York, NY, USA, 1984; pp. 45–74. [CrossRef]
43. Bowman, K.F.; Fox, J.; Sekiya, J.K. A clinically relevant review of hip biomechanics. *Arthrosc. J. Arthrosc. Relat. Surg. Off. Publ. Arthrosc. Assoc. North Am. Int. Arthrosc. Assoc.* **2010**, *26*, 1118–1129. [CrossRef] [PubMed]
44. Byrne, D.P.; Mulhall, K.J.; Baker, J.F. Anatomy & Biomechanics of the Hip. *Open Sports Med. J.* **2010**, *4*, 51–57. [CrossRef]
45. Shapira, J.; Chen, S.L.; Rosinsky, P.J.; Maldonado, D.R.; Meghpara, M.; Lall, A.C.; Domb, B.G. The effect of postoperative femoral offset on outcomes after hip arthroplasty: A systematic review. *J. Orthop.* **2020**, *22*, 5–11. [CrossRef]
46. Rüdiger, H.A.; Guillemin, M.; Latypova, A.; Terrier, A. Effect of changes of femoral offset on abductor and joint reaction forces in total hip arthroplasty. *Arch. Orthop. Trauma Surg.* **2017**, *137*, 1579–1585. [CrossRef]
47. Wang, G.; Guo, A.; Zhang, Y.; Qiang, H.; Yu, H.; Diao, N.; Ma, L.; Zhang, Y.; Zhao, E. Measurement of the relative position of the femoral head center, greater trochanter, and lesser trochanter. *Ann. Palliat. Med.* **2021**, *10*, 11524–11528. [CrossRef]
48. Murray, D.W. The definition and measurement of acetabular orientation. *J. Bone Jt. Surgery. Br. Vol.* **1993**, *75*, 228–232. [CrossRef]
49. Udomkiat, P.; Dorr, L.D.; Wan, Z. Cementless hemispheric porous-coated sockets implanted with press-fit technique without screws: Average ten-year follow-up. *J. Bone Jt. Surgery. Am. Vol.* **2002**, *84*, 1195–1200. [CrossRef]
50. Schmalzried, T.P.; Guttmann, D.; Grecula, M.; Amstutz, H.C. The relationship between the design, position, and articular wear of acetabular components inserted without cement and the development of pelvic osteolysis. *J. Bone Jt. Surg.* **1994**, *76*, 677–688. [CrossRef]
51. Kennedy, J.G.; Rogers, W.B.; Soffe, K.E.; Sullivan, R.J.; Griffen, D.G.; Sheehan, L.J. Effect of Acetabular Component Orientation on Recurrent Dislocation, Pelvic Osteolysis, Polyethylene Wear, and Component Migration. Technical Report 5. *J. Arthroplast.* **1998**, *13*, 530–534. [CrossRef]
52. Hirakawa, K.; Mitsugi, N.; Koshino, T.; Saito, T.; Hirasawa, Y.; Kubo, T. Effect of Acetabular Cup Position and Orientation in Cemented Total Hip Arthroplasty. *Clin. Orthop. Relat. Res.* **2001**, *388*, 135–142. [CrossRef] [PubMed]
53. Wan, Z.; Boutary, M.; Dorr, L.D. The Influence of Acetabular Component Position on Wear in Total Hip Arthroplasty. *J. Arthroplast.* **2008**, *23*, 51–56. [CrossRef] [PubMed]
54. Patil, S.; Bergula, A.; Chen, P.C.; Colwell, C.W.; D'Lima, D.D. Polyethylene wear and acetabular component orientation. *J. Bone Jt. Surgery. Am. Vol.* **2003**, *85* (Suppl. S4), 56–63. [CrossRef] [PubMed]
55. Enneking, W.; Dunham, W.; Gebhardt, M.; Malawar, M.; Pritchard, D. A system for the classification of skeletal resections. *Musculoskelet. Surg.* **1990**, *75*, 217–240.
56. Council Directive 93/42/EEC of 14 June 1993 Concerning Medical Devices. OJ L 169, 12.7.1993, p. 1–43. Available online: https://eur-lex.europa.eu/legal-content/EN/TXT/PDF/?uri=CELEX:31993L0042 (accessed on 13 September 2024).
57. *ISO 5832-3:2021*; Implants for surgery—Metallic materials. ISO: Geneva, Switzerland, 2021.
58. *ASTM F136-13(2021)e1*; Standard Specification for Wrought Titanium-6Aluminum-4Vanadium ELI (Extra Low Interstitial) Alloy for Surgical Implant Applications (UNS R56401). ASTM: West Conshohocken, PA, USA, 2021.
59. Li, S.; Li, X.; Hou, W.; Nune, K.C.; Misra, R.D.K.; Correa-Rodriguez, V.L.; Guo, Z.; Hao, Y.; Yang, R.; Murr, L.E. Fabrication of open-cellular (porous) titanium alloy implants: Osseointegration, vascularization and preliminary human trials. *Sci. China Mater.* **2018**, *61*, 525–536. [CrossRef]
60. Plecko, M.; Sievert, C.; Andermatt, D.; Frigg, R.; Kronen, P.; Klein, K.; Stübinger, S.; Nuss, K.; Bürki, A.; Ferguson, S.; et al. Osseointegration and biocompatibility of different metal implants—A comparative experimental investigation in sheep. *BMC Musculoskelet. Disord.* **2012**, *13*, 32. [CrossRef]
61. Wu, G.; Siegler, S.; Allard, P.; Kirtley, C.; Leardini, A.; Rosenbaum, D.; Whittle, M.; D'Lima, D.D.; Cristofolini, L.; Witte, H.; et al. ISB recommendation on definitions of joint coordinate system of various joints for the reporting of human joint motion—Part I: Ankle, hip, and spine. *J. Biomech.* **2002**, *35*, 543–548. [CrossRef]
62. Cappozzo, A.; Catani, F.; Della Croce, U.; Leardini, A. Position and orientation in space of bones during movement: Anatomical frame definition and determination. *Clin. Biomech.* **1995**, *10*, 171–178. [CrossRef]
63. Durastanti, G.; Belvedere, C.; Ruggeri, M.; Donati, D.M.; Spazzoli, B.; Leardini, A. A Pelvic Reconstruction Procedure for Custom-Made Prosthesis Design of Bone Tumor Surgical Treatments. *Appl. Sci.* **2022**, *12*, 1654. [CrossRef]
64. Li, D.X.; Ead, M.S.; Duke, K.K.; Jaremko, J.L.; Westover, L. Quantitative analysis of regional specific pelvic symmetry. *Med. Biol. Eng. Comput.* **2021**, *59*, 369–381. [CrossRef]
65. Grood, E.S.; Suntay, W.J. A joint coordinate system for the clinical description of three-dimensional motions: Application to the knee. *J. Biomech. Eng.* **1983**, *105*, 136–144. [CrossRef] [PubMed]
66. Sun, F. Affine_fit(X), MATLAB Central File Exchange. 2024. Available online: https://www.mathworks.com/matlabcentral/fileexchange/60502-affine_fit-x (accessed on 11 November 2023).
67. Callanan, M.C.; Jarrett, B.; Bragdon, C.R.; Zurakowski, D.; Rubash, H.E.; Freiberg, A.A.; Malchau, H. The john charnley award: Risk factors for cup malpositioning: Quality improvement through a joint registry at a tertiary hospital. *Clin. Orthop. Relat. Res.* **2011**, *469*, 319–329. [CrossRef] [PubMed]

68. Lewinnek, G.E.; Lewis, J.L.; Tarr, R.; Compere, C.L.; Zimmerman, J.R. Dislocations after total hip-replacement arthroplasties. *J. Bone Jt. Surgery. Am. Vol.* **1978**, *60*, 217–220. [CrossRef]
69. Seidel, G.K.; Marchinda, D.M.; Dijkers, M.; Soutas-Little, R.W. Hip joint center location from palpable bony landmarks—A cadaver study. *J. Biomech.* **1995**, *28*, 995–998. [CrossRef]
70. Bjarnason, J.A.; Reikeras, O. Changes of center of rotation and femoral offset in total hip arthroplasty. *Ann. Transl. Med.* **2015**, *3*, 355. [CrossRef]
71. Cassidy, K.A.; Noticewala, M.S.; Macaulay, W.; Lee, J.H.; Geller, J.A. Effect of Femoral Offset on Pain and Function After Total Hip Arthroplasty. *J. Arthroplast.* **2012**, *27*, 1863–1869. [CrossRef]
72. Durand-Hill, M.; Henckel, J.; Satchithananda, K.; Sabah, S.; Hua, J.; Hothi, H.; Langstaff, R.J.; Skinner, J.; Hart, A. Calculating the hip center of rotation using contralateral pelvic anatomy. *J. Orthop. Res.* **2016**, *34*, 1077–1083. [CrossRef]
73. Hetsroni, I.; Poultsides, L.; Bedi, A.; Larson, C.M.; Kelly, B.T. Anterior inferior iliac spine morphology correlates with hip range of motion: A classification system and dynamic model hip. *Clin. Orthop. Relat. Res.* **2013**, *471*, 2497–2503. [CrossRef]
74. Langridge, B.; Momin, S.; Coumbe, B.; Woin, E.; Griffin, M.; Butler, P. Systematic Review of the Use of 3-Dimensional Printing in Surgical Teaching and Assessment. *J. Surg. Educ.* **2018**, *75*, 209–221. [CrossRef]
75. Barber, S.R.; Kozin, E.D.; Dedmon, M.; Lin, B.M.; Lee, K.; Sinha, S.; Black, N.; Remenschneider, A.K.; Lee, D.J. 3D-printed pediatric endoscopic ear surgery simulator for surgical training. *Int. J. Pediatr. Otorhinolaryngol.* **2016**, *90*, 113–118. [CrossRef]
76. Yang, M.; Li, C.; Li, Y.; Zhao, Y.; Wei, X.; Zhang, G.; Fan, J.; Ni, H.; Chen, Z.; Bai, Y.; et al. Application of 3D rapid prototyping technology in posterior corrective surgery for Lenke 1 adolescent idiopathic scoliosis patients. *Medicine* **2015**, *94*, e582. [CrossRef] [PubMed]
77. Clement, N.D.; Patrick-Patel, R.S.; MacDonald, D.; Breusch, S.J. Total hip replacement: Increasing femoral offset improves functional outcome. *Arch. Orthop. Trauma Surg.* **2016**, *136*, 1317–1323. [CrossRef] [PubMed]
78. Worlicek, M.; Messmer, B.; Grifka, J.; Renkawitz, T.; Weber, M. Restoration of leg length and offset correlates with trochanteric pain syndrome in total hip arthroplasty. *Sci. Rep.* **2020**, *10*, 7107. [CrossRef] [PubMed]
79. Sun, L.; Song, W.; Zhang, Z.; Xu, Z.; Sun, M.; Gao, G.; Jiang, H.; Ju, C. Femoral offset restoration affects the early outcome of revision in patients with periprosthetic femoral fractures of Vancouver B2—A single-center retrospective cohort study. *BMC Musculoskelet. Disord.* **2023**, *24*, 567. [CrossRef] [PubMed]
80. D'Lima, D.D.; Chen, P.C.; Colwell, C.W. Optimizing Acetabular Component Position to Minimize Impingement and Reduce Contact Stress. *J. Bone Jt. Surg. -Am. Vol.* **2001**, *83*, 87–91. [CrossRef] [PubMed]
81. Robinson, R.P.; Simonian, P.T.; Gradisar, I.M.; Ching, R.P. Joint Motion and Surface Contact Area Related To Component Position In Total Hip Arthroplasty. *J. Bone Jt. Surgery. Br. Vol.* **1997**, *79-B*, 140–146. [CrossRef]
82. Nees, T.A.; Mueller, C.T.; Innmann, M.M.; Spranz, D.M.; Westhauser, F.; Renkawitz, T.; Reiner, T.; Walker, T. Assessment Accuracy of 2D vs. 3D Imaging for Custom-Made Acetabular Implants in Revision Hip Arthroplasty. *J. Pers. Med.* **2024**, *14*, 808. [CrossRef]
83. Baauw, M.; van Hellemondt, G.G.; van Hooff, M.L.; Spruit, M. The accuracy of positioning of a custom-made implant within a large acetabular defect at revision arthroplasty of the hip. *Bone Jt. J.* **2015**, *97-B*, 780–785. [CrossRef]
84. Holzapfel, B.M.; Pilge, H.; Prodinger, P.M.; Toepfer, A.; Mayer-Wagner, S.; Hutmacher, D.W.; von Eisenhart-Rothe, R.; Rudert, M.; Gradinger, R.; Rechl, H. Customised osteotomy guides and endoprosthetic reconstruction for periacetabular tumours. *Int. Orthop.* **2014**, *38*, 1435–1442. [CrossRef]
85. Wang, B.; Hao, Y.; Pu, F.; Jiang, W.; Shao, Z. Computer-aided designed, three dimensional-printed hemipelvic prosthesis for peri-acetabular malignant bone tumour. *Int. Orthop.* **2018**, *42*, 687–694. [CrossRef]
86. Zhu, Y.; Babazadeh-Naseri, A.; Dunbar, N.J.; Brake, M.R.; Zandiyeh, P.; Li, G.; Leardini, A.; Spazzoli, B.; Fregly, B.J. Finite element analysis of screw fixation durability under multiple boundary and loading conditions for a custom pelvic implant. *Med. Eng. Phys.* **2023**, *111*, 103930. [CrossRef] [PubMed]
87. Maresca, J.A.; DeMel, D.C.; Wagner, G.A.; Haase, C.; Geibel, J.P. Three-Dimensional Bioprinting Applications for Bone Tissue Engineering. *Cells* **2023**, *12*, 1230. [CrossRef] [PubMed]
88. Fan, D.; Liu, Y.; Wang, Y.; Wang, Q.; Guo, H.; Cai, Y.; Song, R.; Wang, X.; Wang, W. 3D printing of bone and cartilage with polymer materials. *Front. Pharmacol.* **2022**, *13*, 1044726. [CrossRef] [PubMed]
89. McGraw, K.O.; Wong, S.P. Forming inferences about some intraclass correlation coefficients. *Psychol. Methods* **1996**, *1*, 30–46. [CrossRef]
90. Salarian, A. Intraclass Correlation Coefficient (ICC), MATLAB Central File Exchange, 2024. Available online: https://www.mathworks.com/matlabcentral/fileexchange/22099-intraclass-correlation-coefficient-icc (accessed on 13 September 2024).